Table 1. Gene Ontology Analysis of 335 Human Genes Upregulated in 201B7-NS-Grafted Spinal Cord

GO Accession	GO Term	Corrected p Value
GO:0045202	synapse	7.05E-08
GO:0007399	nervous system development	3.56E-06
GO:0007267	cell-cell signaling	7.69E-06
GO:0019226	transmission of nerve impulse	4.68E-04
GO:0043005	neuron projection	1.76E-03
GO:0030182	neuron differentiation	1.26E-02
GO:0007154	cell communication	1.26E-02
GO:0048699	generation of neurons	1.40E-02
GO:0022008	neurogenesis	1.91E-02
GO:0050806	positive regulation of synaptic transmission	3.52E-02
GO:0050804	regulation of synaptic transmission	4.19E-02
GO:0007417	central nervous system development	4.80E-02
GO:0051971	positive regulation of transmission of nerve impulse	4.80E-02

See also Table S2.

number of mesenchyme-associated terms, including "mesenchymal cell differentiation," "mesenchymal cell development," and "epithelial to mesenchymal transition" (Table 2). These terms were also identified in a comparison of 253G1 and 201B7 NS cells, suggesting that 253G1-NS cells were more prone to undergo EMT (Table S3). Furthermore, the mRNA-seq data revealed that EMT-related genes such as *LEF1*, *BMP2*, *HGF*, *SNAI1*, *SNAI2*, *TWIST1*, and *TWIST2* (as suggested by GO analysis and previous reports [Moody et al., 2005; Yang et al., 2004]) were significantly upregulated in the 253G1-NS/TP-103d group relative to the 201B7-NS/TP-103d group (Figures 4F–4L). We also evaluated the expression of *SNAI1*, *SNAI2*, *TWIST1*, and *TWIST2* mRNAs in 201B7-NSs and 253G1-NSs prior to transplantation (Figures 4M–4P). Expression of *SNAI2*, *TWIST1*, and *TWIST2* was significantly higher in 253G1-NSs than in 201B7-NSs (Figures 4N–4P), whereas *SNAI1* expression was significantly lower in 253G1-NSs than in 201B7-NSs (Figure 4M). Furthermore, we evaluated the signal transducer and activator of transcription 3 (STAT3), extracellular-signal-regulated kinase (ERK) and v-akt murine thymoma viral oncogene (AKT) pathways, which are involved in tumor maintenance. Specifically, we performed immunohistochemical analyses to monitor the levels of tyrosine 705-phosphorylated STAT3 (p-STAT3), tyrosine 202/204-phosphorylated ERK1/2 (p-ERK1/2), and serine 473-phosphorylated AKT (p-AKT). We observed p-STAT3$^+$ cells (Figures 4Q–4S), but no p-ERK1/2$^+$ or p-AKT$^+$ cells, in the 253G1-NS/TP-103d group.

Ingenuity Pathway Analysis Revealed Pathways that Differed Significantly between 253G1-NS and 201B7-NS Transplantation

We used Ingenuity Pathway Analysis (IPA) to identify pathways differentially expressed between the 253G1-NS/TP-103d and 201B7-NS/TP-103d groups. IPA detected a total of 56 significantly altered ($p < 0.05$) pathways. Figure 5 shows the ten most altered pathways, all of which were significantly upregulated in the 253G1-NS/TP-103d group relative to iPSC-NSs prior to transplantation.

DISCUSSION

Because we generated the human iPSC clone 253G1 without introducing *c-MYC*, we initially speculated that

(C) Principal-component analysis (PCA) of human gene-expression data. x axis, component 1 (41.03%); y axis, component 2 (24.21%); z axis, component 3 (13.88%).
(D) Two-dimensional PCA of human gene expression data. x axis, component 1 (41.03%); y axis, component 2 (24.21%).
(E) Venn diagram of human genes whose expression increased in the 253G1-NS/TP-103d and 201B7-NS/TP-103d groups relative to 253G1-NSs and 201B7-NSs. Color key: red, 692 genes highly expressed in the 253G1-NS/TP-103d group; blue, 335 genes highly expressed in the 201B7-NS/TP-103d group; purple, 1,023 genes highly expressed in both the 253G1- and 201B7-NS/TP-103d groups.
(F–L) EMT-related human gene expression in 253G1- and 201B7-NSs and the 253G1- and 201B7-NS/TP-103d groups. Values represent the means ± SEM (n = 1 each in the human iPSC-NS, n = 2 for 201B7-NS/TP-103d, and n = 3 for 253G1-NS/TP-103d; n indicates the number of independent experiments).
(M–P) The expression of *SNAI1*, *SNAI2*, *TWIST1*, and *TWIST2* mRNA in 201B7-NSs and 253G1-NSs was analyzed by RT-PCR. Data are presented as expression levels relative to the control (the U87 human glioblastoma cell line). Values represent the means ± SEM (n = 3 independent experiments).
(Q) Representative H&E image of the mid-sagittal section 103 days after transplantation.
(R) p-STAT3-stained image of the adjacent section of (Q). Arrow, lesion epicenter; arrowhead, distribution of grafted 253G1-NSs.
(S) Boxed area in (R).
Scale bar, 1,000 μm in (Q) and (R), 100 μm in (S). *$p < 0.05$, **$p < 0.01$. See also the mRNA-seq read distribution in Table S1.

Table 2. Gene Ontology Analysis of 692 Human Genes Upregulated in 253G1-NS-Grafted Spinal Cord

GO Accession	GO Term	Corrected p Value
GO:0030198	extracellular matrix organization and biogenesis	2.29E-16
GO:0001501	skeletal development	1.29E-14
GO:0043062	extracellular structure organization and biogenesis	2.67E-13
GO:0001568	blood vessel development	1.88E-12
GO:0001944	vasculature development	3.51E-12
GO:0030199	collagen fibril organization	5.50E-08
GO:0014031	mesenchymal cell development	2.78E-07
GO:0048762	mesenchymal cell differentiation	4.84E-07
GO:0001525	Angiogenesis	2.81E-06
GO:0048514	blood vessel morphogenesis	3.02E-06
GO:0001503	ossification	1.74E-05
GO:0031214	biomineral formation	1.89E-05
GO:0014032	neural crest cell development	5.94E-04
GO:0014033	neural crest cell differentiation	7.55E-04
GO:0007517	muscle development	3.04E-03
GO:0042127	regulation of cell proliferation	4.84E-03
GO:0001837	epithelial to mesenchymal transition	2.02E-02

See also Table S3.

253G1-NSs would be less tumorigenic than 201B7-NSs. Therefore, we performed transplantation of 253G1-NSs to treat SCI in adult NOD-SCID mice. Like the 201B7-NSs, the grafted 253G1-NSs differentiated into three neural lineages, reconstructed local circuitry, and promoted angiogenesis as well as axonal regrowth (data not shown). Thus, 253G1-NS transplantation promoted motor function recovery after SCI in NOD-SCID mice.

When considering the clinical use of iPSC-NSs, it is important to address safety issues, especially with regard to tumorigenicity. To this end, we extended the observation period after transplantation. Previously, we reported that 201B7-NS-grafted mice maintained functional recovery until 103 days post-transplantation, and confirmed that 201B7-NSs were non-tumorigenic based on histological findings (Nori et al., 2011). Here, we found that 253G1-NS-grafted mice exhibited temporary motor function recovery for up to 47 days post-transplantation; however, this was followed by a gradual deterioration in motor function, along with grafted cell proliferation and tumor development. Bioluminescence imaging revealed that the photon count of the grafted cells increased more than 10-fold from the initial value by 103 days after transplantation. These tumors were negative for the pluripotency marker NANOG. Tumor size correlated with the proportion of Nestin$^+$ cells in the graft at 103 days post-transplantation. Previously, we showed that after 201B7-NS transplantation, the proportion of grafted cells that were Nestin$^+$ decreased from 10.7% ± 2.2% at 47 days to 7.5% ± 1.0% at 103 days post-transplantation, resulting in no evidence of tumorigenicity (Nori et al., 2011). By contrast, the proportion of Nestin$^+$ cells increased from 19.6% ± 0.5% at 47 days to 33.1% ± 7.4% at 103 days after 253G1-NS transplantation, suggesting that differentiation-resistant Nestin$^+$ cells proliferated over time and formed tumors. Consistent with this, the proportion of Ki-67$^+$ cells significantly increased from 1.7% ± 0.17% at 47 days to 3.0% ± 0.2% at 103 days after 253G1-NS transplantation, which is significantly higher than what was observed after 201B7-NS transplantation. These findings suggest that the proportion of proliferating cells increased over time and induced tumor formation in 253G1-NS-grafted mice in the long term.

Tumor diameter exhibited no significant correlation with the proportion of OCT4$^+$/HNu$^+$ cells. Instead, the proportion of grafted cells that were OCT4$^+$ was solely dependent on the post-transplantation observation period. In our previous study, we observed no evidence of OCT4$^+$/HNu$^+$ cells or tumor formation in 201B7-NS-grafted mice after long-term observation (Nori et al., 2011). It is likely that the chronologically increasing OCT4 expression in the grafted 253G1-NSs is related to tumor formation, consistent with the results of RT-PCR, which showed that the expression of *OCT4*-Tg at 103 days post-transplantation was significantly higher than that in untransplanted 253G1-NSs. OCT4 is a key regulator of self-renewal and plays a critical role in maintaining ESC pluripotency (Niwa, 2007). In addition, OCT4 is sometimes re-expressed in somatic cells during carcinogenesis (Monk and Holding, 2001). OCT4 is also highly expressed in human gliomas and glioma cell lines, and OCT4 overexpression in glioma cells induces Nestin expression by inhibiting glioma cell differentiation (Du et al., 2009; Ikushima et al., 2011). These findings are consistent with the results we describe here, even though the tumors observed in the present study were not pathologically identical to gliomas. We also observed that *KLF4*-Tg was activated in 253G1-NSs, and that its expression increased after transplantation. KLF4 is highly expressed in primary breast ductal carcinoma and oral squamous carcinoma (Foster et al., 2005; Pandya et al.,

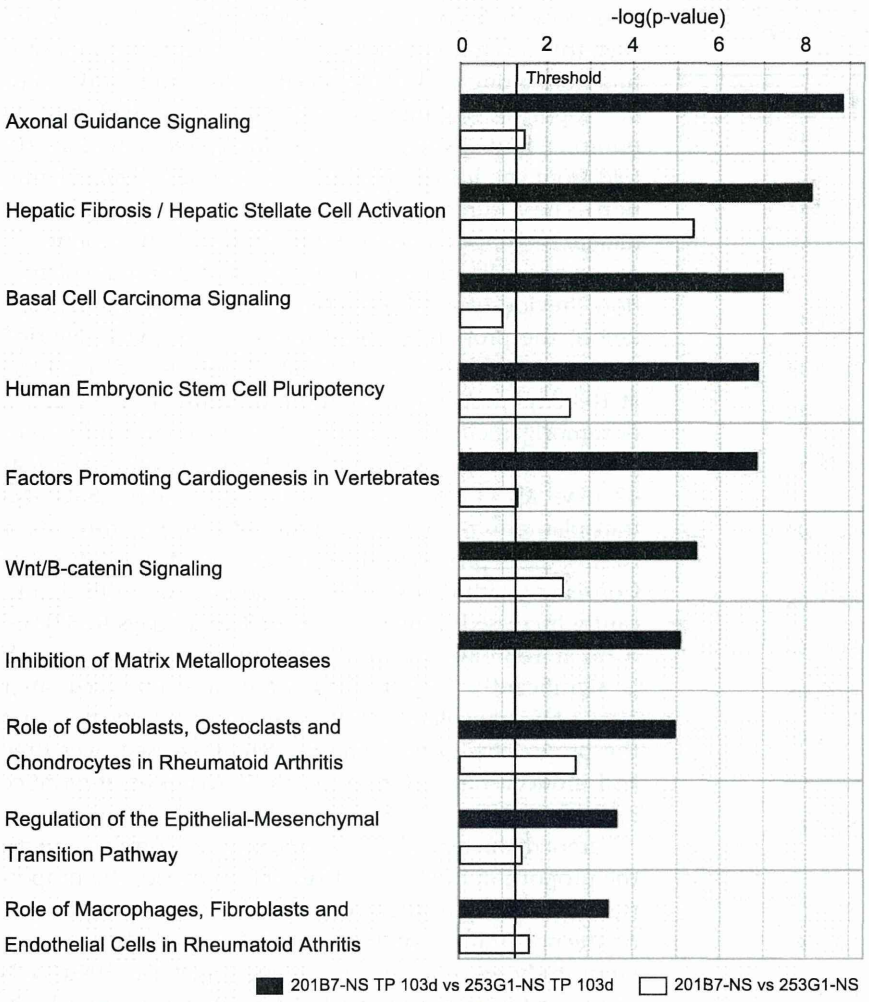

Figure 5. The Most Significantly Altered Common Pathways after Transplantation of 253G1- and 201B7-NSs, as Revealed by Ingenuity Pathway Analysis

Canonical pathway analysis identified the pathways from the Ingenuity Pathway Analysis library that were significantly enriched in the data set. Only genes that showed a fold change $\geq$ 3.0 were considered in this analysis. The black bars show the human gene set in the 253G1-NS/TP-103d group versus the 201B7-NS/TP-103d group. The white bars show the comparison of the human gene set in 253G1-NSs versus 201B7-NSs in the same pathway. Bars represent the logarithmic values (log_{10}) of the significance level (p); the solid line corresponds to the threshold of p = 0.05.

2004). Previous reports also showed that KLF4 overexpression promotes self-renewal in ESCs (Li et al., 2005), and KLF4 is an essential reprogramming factor that functions by binding at *Oct4* loci to initiate *Oct4* transcription and complete the reprogramming process (Wei et al., 2013). These results suggest that KLF4 plays an important role in maintaining PSCs, and that the tumor formation we observed could be related to *KLF4*-Tg activation.

In a previous study, the molecular properties of engrafted NS/PCs changed dramatically depending on the spinal cord microenvironment (Kumamaru et al., 2012). Here, we analyzed the changes in the microenvironment of mouse spinal cord tissues affected by iPSC-NS transplantation. We observed no significant differences in the mouse gene-expression profiles of spinal cord tissues among the 253G1-NS/TP, 201B7-NS/TP, and control groups, suggesting that mouse gene expression did not widely affect tumorigenesis in grafted iPSC-NSs. However, human gene-expression profiles from the 253G1- and 201B7-NS/TP groups differed in a time-dependent manner, which may have been related to tumor formation in the 253G1-NS/TP group. GO analysis revealed increased progression of EMT in the 253G1-NS and 253G1-NS/TP groups relative to the 201B7-NS and 201B7-NS/TP groups.

During EMT, epithelial cells lose their epithelial characteristics and acquire the properties of migratory mesenchymal cells. This process is associated with the early stages of carcinogenesis, cancer invasion, and recurrence (Hay, 1995; Thiery, 2002). Brain tumors, including some human gliomas, also contain stem-like cells with both neural and mesenchymal potential that are implicated in both tumor progression and invasiveness (Ricci-Vitiani et al., 2008). STAT3 is frequently overexpressed in cancers, including gliomas (Abou-Ghazal et al., 2008), and STAT3 phosphorylation leads to the transcriptional activation of genes involved in processes such as cell proliferation, apoptosis suppression, and angiogenesis (Bowman et al., 2001). Moreover, STAT3 regulates the EMT gene TWIST (Cheng et al., 2008), consistent with the more active EMT progression and

elevated TWIST expression in the 253G1-NS/TP group observed in this study. Mesenchyme-like changes in 253G1-NSs following transplantation may contribute to the biological characteristics of tumor cells derived from parental 253G1-NSs.

IPA revealed upregulation of human ESC pluripotency pathways in post-transplantation 253G1-NSs. This phenomenon might be related to the population of differentiation-resistant Nestin$^+$ cells that proliferated over time and formed tumors. Furthermore, the Wnt/β-catenin signaling pathway was significantly upregulated in the 253G1-NS/TP group. Previous studies showed that Wnt/β-catenin signaling is critical for regulating the self-renewal, proliferation, and differentiation of NS/PCs in the brain (Gong and Huang, 2012), and that this pathway leads to enhanced *TERT* expression in human cancers, resulting in the stabilization of telomeres, a hallmark of tumorigenesis (Hoffmeyer et al., 2012). In part, the tumorigenicity of 253G1-NSs could be related to upregulation of the Wnt/β-catenin signaling pathway. Moreover, consistent with GO analysis, regulation of the EMT pathway was significantly upregulated in the 253G1-NS/TP group relative to the 207B7-NS/TP group.

Recently, several clinical trials of stem-cell-based therapy for SCI using either human NS/PCs (Cummings et al., 2005; Salazar et al., 2010) or human ESC-derived OPCs (Strauss, 2010) have been initiated. Compared with these stem cells, iPSCs raise fewer ethical concerns in certain countries (Nori et al., 2011; Tsuji et al., 2010). On the other hand, the use of iPSC-derived cells risks tumorigenesis (Miura et al., 2009; Tsuji et al., 2010). The present study demonstrates that even unsafe iPSC-NSs can confer therapeutic benefits against SCI, at least in the short term. However, long-term observation is required to assess the safety of iPSC-NSs, because slow-growing tumors could cause motor function to deteriorate over longer periods of time. In the present study, we used retrovirally generated iPSCs (Nakagawa et al., 2008; Takahashi et al., 2007) and showed that activation of *OCT4*- and *KLF4*-Tg might be related to tumor formation. Thus, from a clinical-applications perspective, NS/PCs derived from integration-free iPSCs (Okita et al., 2008, 2011) should be chosen to avoid Tg-induced tumorigenesis. Recently, a pilot clinical study of integration-free iPSC-based therapy for age-related macular degeneration was approved following review by the Japanese government (Garber, 2013; Kamao et al., 2014). As a step toward clinical applications in the SCI field, we have already initiated integration-free iPSC-NS transplantation in the NOD-SCID mouse SCI model. At the same time, transplantation into immune-deficient animals, accompanied by subsequent long-term observation, should be used to determine the safety and effectiveness of these cells (Okano et al., 2013).

EXPERIMENTAL PROCEDURES

Additional details regarding several of the protocols used in this work are provided in Supplemental Experimental Procedures.

Cell Culture, Neural Differentiation, and Lentiviral Transduction

Cell culture, neural differentiation of human iPSCs (253G1), and lentiviral transduction of neurospheres were performed as described previously (Nori et al., 2011; Okada et al., 2008). Briefly, 253G1-derived primary neurospheres were dissociated and infected with lentivirus expressing Venus or ffLuc under the control of the EF promoter. Primary neurospheres were passaged into secondary and tertiary neurospheres. The ffLuc vector enabled detection of grafted cells as strong bioluminescent ffLuc signals in live SCI mice, and as fluorescent Venus signals in fixed spinal cord sections.

Animal Model and Cell Transplantation

Adult female NOD-SCID mice (20–22 g) were anesthetized via intraperitoneal (i.p.) injection of ketamine (100 mg/kg) and xylazine (10 mg/kg). After laminectomy, contusive SCI was induced at the Th10 level using an IH impactor (60 kdyn; Precision Systems and Instrumentation) as described previously (Scheff et al., 2003). Nine days after SCI, 253G1-NSs (5×10^5 cells) were transplanted into the lesion epicenter of each mouse (n = 37) using a glass micropipette and stereotaxic injector (KDS310; Muromachi Kikai). The 253G1-NSs were transplanted at approximately the same time as the PBS injection and 201B7-NS transplantation described in our previous report (Nori et al., 2011).

Bioluminescence Imaging

A Xenogen-IVIS spectrum-cooled, charge-coupled device optical macroscopic imaging system (Summit Pharmaceuticals International) was used for bioluminescence imaging to confirm the survival of the grafted cells as previously described (Itakura et al., 2014; Okada et al., 2005; Takahashi et al., 2011). Monitoring was performed for 103 days post-transplantation.

Motor Function and Histological Analyses

Motor function was evaluated using the BMS, Rotarod apparatus (Muromachi Kikai), and DigiGait system (Mouse Specifics). For histological analyses, the animals were anesthetized and transcardially perfused with 4% paraformaldehyde (pH 7.4). Spinal cords were removed and sectioned in the sagittal/axial plane on a cryostat. All motor function and histological analyses were conducted by observers blinded to the treatment conditions. All animal experiments (approval number 09169) were performed under the control of the Keio University Institutional Animal Care and Use Committee in accordance with the Institutional Guidelines on Animal Experimentation at Keio University, the Japanese Government Law Concerning the Protection and Control of Animals, and the Japanese Government Notification of Feeding and Safekeeping of Animals, and approved by the ethics committee of Keio University (IRB approval number 09091-8).

RT-PCR

RNA isolation and RT-PCR were performed as previously described (Nori et al., 2011; Okada et al., 2008).

Transcriptome Analysis

Total RNA from each sample was purified as previously described (Okada et al., 2008). mRNA libraries were prepared according to the TruSeq RNA sample prep kit protocol and sequenced using a Genome Analyzer IIx (Illumina). Mouse and human mRNA sequences were separated using Xenome software (Conway et al., 2012), and separated mRNA-seq data were mapped to the corresponding genomic DNA sequences (human [hg19] and mouse [mm9]) using TopHat software (Trapnell et al., 2009). The mapped sequences were normalized by trimmed mean of M values (TMM) and analyzed using Avadis NGS software (Agilent Technologies). All software used default parameters. For principal component analysis (PCA) and clustering analysis, the normalized data were narrowed down to 13,693 genes using a cutoff value for expression levels (reads per kilobase of exon per million mapped reads [RPKM] > 100). A Venn diagram was constructed to visualize the 1,715 genes that were upregulated in the 253G1-NS/TP-103d group and the 1,358 genes that were upregulated in the 201B7-NS/TP-103d group (RPKM > 100, fold change > 5.0 versus each NS group). GO analysis was performed using gene lists from the overlapping area, as well as from each separate area, in the Venn diagram. For GO analysis, p values were calculated using Fisher's exact test. Subsequently corrected p values were applied for multiple testing corrections using the Benjamini-Yekutieli method with a cutoff at $p = 0.05$. Pathway analysis was performed via IPA (Ingenuity Systems) using genes that were up- or downregulated in the 253G1-NS/TP-103d group versus the 201B7-NS/TP-103d group, as well as in 253G1-NS versus 201B7-NS (RPKM > 100, fold-change > 3.0). The genes were overlaid on the Ingenuity Knowledge Database and networks were algorithmically generated based on their connectivity. The p values were determined using Fisher's exact test and $p = 0.05$ was interpreted as indicating statistical significance.

Statistical Analyses

An unpaired, two-tailed Student's t test was used to assess the 253G1-NS differentiation efficacy. One-way ANOVA followed by the Tukey-Kramer test for multiple comparisons was used for the Ki-67, Rotarod, and DigiGait analyses. Repeated-measures, two-way ANOVA followed by the Tukey-Kramer test was used for the BMS analysis. The Kruskal-Wallis non-parametric test and Scheffe's test were used to analyze tumor diameter and the percentage of HNu^+ grafted cells that were $Nestin^+$, $Ki\text{-}67^+$, or $OCT4^+$. Statistical significance was determined as $^*p < 0.05$, $^{**}p < 0.01$.

SUPPLEMENTAL INFORMATION

Supplemental Information includes Supplemental Experimental Procedures, two figures, and three tables and can be found with this article online at http://dx.doi.org/10.1016/j.stemcr.2015.01.006.

ACKNOWLEDGMENTS

We thank A. Iwanami, S. Kaneko, K. Fujiyoshi, O. Tsuji, A. Yasuda, Y. Takahashi, S. Kawabata, Y. Nishiyama, T. Iida, S. Shibata, T. Harada, S. Miyao, and H.J. Okano for technical assistance and scientific discussions, and H. Saya, M. Ko, M. Jakt, and K. Horiuchi for critical readings of the manuscript. We also thank S. Yamanaka and M. Nakagawa for the human iPSC clones (253G1 and 201B7). The p-STAT3, p-ERK1/2, and p-AKT antibodies were kindly provided by N. Onishi. This work was supported by grants from the JST-CIRM collaborative program; Grants-in-Aid for Scientific Research from JSPS and the Ministry of Education, Culture, Sports, Science, and Technology of Japan (MEXT); Research Center Network for Realization of Regenerative Medicine from by the Japan Science and Technology Agency (JST); the Kanrinmaru Project (Keio University); Research Fellowships for Young Scientists from the Japan Society for the Promotion of Science; Keio Gijuku Academic Development Funds; and a Grant-in-Aid for Scientific Research on Innovative Areas (Comprehensive Brain Science Network) from the MEXT.

Received: February 21, 2014
Revised: January 9, 2015
Accepted: January 12, 2015
Published: February 12, 2015

REFERENCES

Abou-Ghazal, M., Yang, D.S., Qiao, W., Reina-Ortiz, C., Wei, J., Kong, L.Y., Fuller, G.N., Hiraoka, N., Priebe, W., Sawaya, R., and Heimberger, A.B. (2008). The incidence, correlation with tumor-infiltrating inflammation, and prognosis of phosphorylated STAT3 expression in human gliomas. Clin. Cancer Res. *14*, 8228–8235.

Bowman, T., Broome, M.A., Sinibaldi, D., Wharton, W., Pledger, W.J., Sedivy, J.M., Irby, R., Yeatman, T., Courtneidge, S.A., and Jove, R. (2001). Stat3-mediated Myc expression is required for Src transformation and PDGF-induced mitogenesis. Proc. Natl. Acad. Sci. USA *98*, 7319–7324.

Bradford, J.R., Farren, M., Powell, S.J., Runswick, S., Weston, S.L., Brown, H., Delpuech, O., Wappett, M., Smith, N.R., Carr, T.H., et al. (2013). RNA-seq differentiates tumour and host mRNA expression changes induced by treatment of human tumour xenografts with the VEGFR tyrosine kinase inhibitor Cediranib. PLoS ONE *8*, e66003.

Cheng, G.Z., Zhang, W.Z., Sun, M., Wang, Q., Coppola, D., Mansour, M., Xu, L.M., Costanzo, C., Cheng, J.Q., and Wang, L.H. (2008). Twist is transcriptionally induced by activation of STAT3 and mediates STAT3 oncogenic function. J. Biol. Chem. *283*, 14665–14673.

Conway, T., Wazny, J., Bromage, A., Tymms, M., Sooraj, D., Williams, E.D., and Beresford-Smith, B. (2012). Xenome—a tool for classifying reads from xenograft samples. Bioinformatics *28*, i172–i178.

Cummings, B.J., Uchida, N., Tamaki, S.J., Salazar, D.L., Hooshmand, M., Summers, R., Gage, F.H., and Anderson, A.J. (2005). Human neural stem cells differentiate and promote locomotor

recovery in spinal cord-injured mice. Proc. Natl. Acad. Sci. USA *102*, 14069–14074.

Du, Z., Jia, D., Liu, S., Wang, F., Li, G., Zhang, Y., Cao, X., Ling, E.A., and Hao, A. (2009). Oct4 is expressed in human gliomas and promotes colony formation in glioma cells. Glia *57*, 724–733.

Erceg, S., Ronaghi, M., Oria, M., Roselló, M.G., Aragó, M.A., Lopez, M.G., Radojevic, I., Moreno-Manzano, V., Rodríguez-Jiménez, F.J., Bhattacharya, S.S., et al. (2010). Transplanted oligodendrocytes and motoneuron progenitors generated from human embryonic stem cells promote locomotor recovery after spinal cord transection. Stem Cells *28*, 1541–1549.

Falk, A., Koch, P., Kesavan, J., Takashima, Y., Ladewig, J., Alexander, M., Wiskow, O., Tailor, J., Trotter, M., Pollard, S., et al. (2012). Capture of neuroepithelial-like stem cells from pluripotent stem cells provides a versatile system for in vitro production of human neurons. PLoS ONE *7*, e29597.

Foster, K.W., Liu, Z., Nail, C.D., Li, X., Fitzgerald, T.J., Bailey, S.K., Frost, A.R., Louro, I.D., Townes, T.M., Paterson, A.J., et al. (2005). Induction of KLF4 in basal keratinocytes blocks the proliferation-differentiation switch and initiates squamous epithelial dysplasia. Oncogene *24*, 1491–1500.

Fujimoto, Y., Abematsu, M., Falk, A., Tsujimura, K., Sanosaka, T., Juliandi, B., Semi, K., Namihira, M., Komiya, S., Smith, A., and Nakashima, K. (2012a). Treatment of a mouse model of spinal cord injury by transplantation of human induced pluripotent stem cell-derived long-term self-renewing neuroepithelial-like stem cells. Stem Cells *30*, 1163–1173.

Fujimoto, Y., Abematsu, M., Falk, A., Tsujimura, K., Sanosaka, T., Juliandi, B., Semi, K., Namihira, M., Komiya, S., Smith, A., and Nakashima, K. (2012b). Treatment of a mouse model of spinal cord injury by transplantation of human iPS cell-derived long-term self-renewing neuroepithelial-like stem cells. Stem Cells *30*, 1163–1173.

Garber, K. (2013). Inducing translation. Nat. Biotechnol. *31*, 483–486.

Gong, A., and Huang, S. (2012). FoxM1 and Wnt/β-catenin signaling in glioma stem cells. Cancer Res. *72*, 5658–5662.

Hara-Miyauchi, C., Tsuji, O., Hanyu, A., Okada, S., Yasuda, A., Fukano, T., Akazawa, C., Nakamura, M., Imamura, T., Matsuzaki, Y., et al. (2012). Bioluminescent system for dynamic imaging of cell and animal behavior. Biochem. Biophys. Res. Commun. *419*, 188–193.

Hay, E.D. (1995). An overview of epithelio-mesenchymal transformation. Acta Anat. (Basel) *154*, 8–20.

Hoffmeyer, K., Raggioli, A., Rudloff, S., Anton, R., Hierholzer, A., Del Valle, I., Hein, K., Vogt, R., and Kemler, R. (2012). Wnt/β-catenin signaling regulates telomerase in stem cells and cancer cells. Science *336*, 1549–1554.

Hofstetter, C.P., Holmström, N.A., Lilja, J.A., Schweinhardt, P., Hao, J., Spenger, C., Wiesenfeld-Hallin, Z., Kurpad, S.N., Frisén, J., and Olson, L. (2005). Allodynia limits the usefulness of intraspinal neural stem cell grafts; directed differentiation improves outcome. Nat. Neurosci. *8*, 346–353.

Ikushima, H., Todo, T., Ino, Y., Takahashi, M., Saito, N., Miyazawa, K., and Miyazono, K. (2011). Glioma-initiating cells retain their tumorigenicity through integration of the Sox axis and Oct4 protein. J. Biol. Chem. *286*, 41434–41441.

Itakura, G., Kobayashi, Y., Nishimura, S., Iwai, H., Takano, M., Iwanami, A., Toyama, Y., Okano, H., and Nakamura, M. (2014). Control of the survival and growth of human glioblastoma grafted into the spinal cord of mice by taking advantage of immunorejection. Cell Transplant. Published online May 9, 2014. http://dx.doi.org/10.3727/096368914X681711.

Iwanami, A., Kaneko, S., Nakamura, M., Kanemura, Y., Mori, H., Kobayashi, S., Yamasaki, M., Momoshima, S., Ishii, H., Ando, K., et al. (2005). Transplantation of human neural stem cells for spinal cord injury in primates. J. Neurosci. Res. *80*, 182–190.

Kamao, H., Mandai, M., Okamoto, S., Sakai, N., Suga, A., Sugita, S., Kiryu, J., and Takahashi, M. (2014). Characterization of human induced pluripotent stem cell-derived retinal pigment epithelium cell sheets aiming for clinical application. Stem Cell Reports *2*, 205–218.

Keirstead, H.S., Nistor, G., Bernal, G., Totoiu, M., Cloutier, F., Sharp, K., and Steward, O. (2005). Human embryonic stem cell-derived oligodendrocyte progenitor cell transplants remyelinate and restore locomotion after spinal cord injury. J. Neurosci. *25*, 4694–4705.

Kobayashi, Y., Okada, Y., Itakura, G., Iwai, H., Nishimura, S., Yasuda, A., Nori, S., Hikishima, K., Konomi, T., Fujiyoshi, K., et al. (2012). Pre-evaluated safe human iPSC-derived neural stem cells promote functional recovery after spinal cord injury in common marmoset without tumorigenicity. PLoS ONE *7*, e52787.

Kumagai, G., Okada, Y., Yamane, J., Nagoshi, N., Kitamura, K., Mukaino, M., Tsuji, O., Fujiyoshi, K., Katoh, H., Okada, S., et al. (2009). Roles of ES cell-derived gliogenic neural stem/progenitor cells in functional recovery after spinal cord injury. PLoS ONE *4*, e7706.

Kumamaru, H., Ohkawa, Y., Saiwai, H., Yamada, H., Kubota, K., Kobayakawa, K., Akashi, K., Okano, H., Iwamoto, Y., and Okada, S. (2012). Direct isolation and RNA-seq reveal environment-dependent properties of engrafted neural stem/progenitor cells. Nat. Commun. *3*, 1140.

Li, Y., McClintick, J., Zhong, L., Edenberg, H.J., Yoder, M.C., and Chan, R.J. (2005). Murine embryonic stem cell differentiation is promoted by SOCS-3 and inhibited by the zinc finger transcription factor Klf4. Blood *105*, 635–637.

Lukovic, D., Valdés-Sanchez, L., Sanchez-Vera, I., Moreno-Manzano, V., Stojkovic, M., Bhattacharya, S.S., and Erceg, S. (2014). Brief report: astrogliosis promotes functional recovery of completely transected spinal cord following transplantation of hESC-derived oligodendrocyte and motoneuron progenitors. Stem Cells *32*, 594–599.

Miura, K., Okada, Y., Aoi, T., Okada, A., Takahashi, K., Okita, K., Nakagawa, M., Koyanagi, M., Tanabe, K., Ohnuki, M., et al. (2009). Variation in the safety of induced pluripotent stem cell lines. Nat. Biotechnol. *27*, 743–745.

Monk, M., and Holding, C. (2001). Human embryonic genes re-expressed in cancer cells. Oncogene *20*, 8085–8091.

Moody, S.E., Perez, D., Pan, T.C., Sarkisian, C.J., Portocarrero, C.P., Sterner, C.J., Notorfrancesco, K.L., Cardiff, R.D., and Chodosh, L.A.

(2005). The transcriptional repressor Snail promotes mammary tumor recurrence. Cancer Cell *8*, 197–209.

Nagai, T., Ibata, K., Park, E.S., Kubota, M., Mikoshiba, K., and Miyawaki, A. (2002). A variant of yellow fluorescent protein with fast and efficient maturation for cell-biological applications. Nat. Biotechnol. *20*, 87–90.

Nakagawa, M., Koyanagi, M., Tanabe, K., Takahashi, K., Ichisaka, T., Aoi, T., Okita, K., Mochiduki, Y., Takizawa, N., and Yamanaka, S. (2008). Generation of induced pluripotent stem cells without Myc from mouse and human fibroblasts. Nat. Biotechnol. *26*, 101–106.

Niwa, H. (2007). How is pluripotency determined and maintained? Development *134*, 635–646.

Nori, S., Okada, Y., Yasuda, A., Tsuji, O., Takahashi, Y., Kobayashi, Y., Fujiyoshi, K., Koike, M., Uchiyama, Y., Ikeda, E., et al. (2011). Grafted human-induced pluripotent stem-cell-derived neurospheres promote motor functional recovery after spinal cord injury in mice. Proc. Natl. Acad. Sci. USA *108*, 16825–16830.

Ogawa, Y., Sawamoto, K., Miyata, T., Miyao, S., Watanabe, M., Nakamura, M., Bregman, B.S., Koike, M., Uchiyama, Y., Toyama, Y., and Okano, H. (2002). Transplantation of in vitro-expanded fetal neural progenitor cells results in neurogenesis and functional recovery after spinal cord contusion injury in adult rats. J. Neurosci. Res. *69*, 925–933.

Okada, Y., Shimazaki, T., Sobue, G., and Okano, H. (2004). Retinoic-acid-concentration-dependent acquisition of neural cell identity during in vitro differentiation of mouse embryonic stem cells. Dev. Biol. *275*, 124–142.

Okada, S., Ishii, K., Yamane, J., Iwanami, A., Ikegami, T., Katoh, H., Iwamoto, Y., Nakamura, M., Miyoshi, H., Okano, H.J., et al. (2005). In vivo imaging of engrafted neural stem cells: its application in evaluating the optimal timing of transplantation for spinal cord injury. FASEB J. *19*, 1839–1841.

Okada, Y., Matsumoto, A., Shimazaki, T., Enoki, R., Koizumi, A., Ishii, S., Itoyama, Y., Sobue, G., and Okano, H. (2008). Spatiotemporal recapitulation of central nervous system development by murine embryonic stem cell-derived neural stem/progenitor cells. Stem Cells *26*, 3086–3098.

Okano, H., Nakamura, M., Yoshida, K., Okada, Y., Tsuji, O., Nori, S., Ikeda, E., Yamanaka, S., and Miura, K. (2013). Steps toward safe cell therapy using induced pluripotent stem cells. Circ. Res. *112*, 523–533.

Okita, K., Nakagawa, M., Hyenjong, H., Ichisaka, T., and Yamanaka, S. (2008). Generation of mouse induced pluripotent stem cells without viral vectors. Science *322*, 949–953.

Okita, K., Matsumura, Y., Sato, Y., Okada, A., Morizane, A., Okamoto, S., Hong, H., Nakagawa, M., Tanabe, K., Tezuka, K., et al. (2011). A more efficient method to generate integration-free human iPS cells. Nat. Methods *8*, 409–412.

Pandya, A.Y., Talley, L.I., Frost, A.R., Fitzgerald, T.J., Trivedi, V., Chakravarthy, M., Chhieng, D.C., Grizzle, W.E., Engler, J.A., Krontiras, H., et al. (2004). Nuclear localization of KLF4 is associated with an aggressive phenotype in early-stage breast cancer. Clin. Cancer Res. *10*, 2709–2719.

Ricci-Vitiani, L., Pallini, R., Larocca, L.M., Lombardi, D.G., Signore, M., Pierconti, F., Petrucci, G., Montano, N., Maira, G., and De Maria, R. (2008). Mesenchymal differentiation of glioblastoma stem cells. Cell Death Differ. *15*, 1491–1498.

Salazar, D.L., Uchida, N., Hamers, F.P., Cummings, B.J., and Anderson, A.J. (2010). Human neural stem cells differentiate and promote locomotor recovery in an early chronic spinal cord injury NOD-scid mouse model. PLoS ONE *5*, e12272.

Scheff, S.W., Rabchevsky, A.G., Fugaccia, I., Main, J.A., and Lumpp, J.E., Jr. (2003). Experimental modeling of spinal cord injury: characterization of a force-defined injury device. J. Neurotrauma *20*, 179–193.

Strauss, S. (2010). Geron trial resumes, but standards for stem cell trials remain elusive. Nat. Biotechnol. *28*, 989–990.

Takahashi, K., Tanabe, K., Ohnuki, M., Narita, M., Ichisaka, T., Tomoda, K., and Yamanaka, S. (2007). Induction of pluripotent stem cells from adult human fibroblasts by defined factors. Cell *131*, 861–872.

Takahashi, Y., Tsuji, O., Kumagai, G., Hara, C.M., Okano, H.J., Miyawaki, A., Toyama, Y., Okano, H., and Nakamura, M. (2011). Comparative study of methods for administering neural stem/progenitor cells to treat spinal cord injury in mice. Cell Transplant. *20*, 727–739.

Thiery, J.P. (2002). Epithelial-mesenchymal transitions in tumour progression. Nat. Rev. Cancer *2*, 442–454.

Trapnell, C., Pachter, L., and Salzberg, S.L. (2009). TopHat: discovering splice junctions with RNA-Seq. Bioinformatics *25*, 1105–1111.

Tsuji, O., Miura, K., Okada, Y., Fujiyoshi, K., Mukaino, M., Nagoshi, N., Kitamura, K., Kumagai, G., Nishino, M., Tomisato, S., et al. (2010). Therapeutic potential of appropriately evaluated safe-induced pluripotent stem cells for spinal cord injury. Proc. Natl. Acad. Sci. USA *107*, 12704–12709.

Wang, S., Bates, J., Li, X., Schanz, S., Chandler-Militello, D., Levine, C., Maherali, N., Studer, L., Hochedlinger, K., Windrem, M., and Goldman, S.A. (2013). Human iPSC-derived oligodendrocyte progenitor cells can myelinate and rescue a mouse model of congenital hypomyelination. Cell Stem Cell *12*, 252–264.

Wei, Z., Gao, F., Kim, S., Yang, H., Lyu, J., An, W., Wang, K., and Lu, W. (2013). Klf4 organizes long-range chromosomal interactions with the oct4 locus in reprogramming and pluripotency. Cell Stem Cell *13*, 36–47.

Yang, J., Mani, S.A., Donaher, J.L., Ramaswamy, S., Itzykson, R.A., Come, C., Savagner, P., Gitelman, I., Richardson, A., and Weinberg, R.A. (2004). Twist, a master regulator of morphogenesis, plays an essential role in tumor metastasis. Cell *117*, 927–939.

Yasuda, A., Tsuji, O., Shibata, S., Nori, S., Takano, M., Kobayashi, Y., Takahashi, Y., Fujiyoshi, K., Hara, C.M., Miyawaki, A., et al. (2011). Significance of remyelination by neural stem/progenitor cells transplanted into the injured spinal cord. Stem Cells *29*, 1983–1994.

Stem Cell Reports
Article

ISSCR

OPEN ACCESS

Involvement of ER Stress in Dysmyelination of Pelizaeus-Merzbacher Disease with *PLP1* Missense Mutations Shown by iPSC-Derived Oligodendrocytes

Yuko Numasawa-Kuroiwa,[1,2] Yohei Okada,[1,3,*] Shinsuke Shibata,[1] Noriyuki Kishi,[1] Wado Akamatsu,[1] Masanobu Shoji,[4] Atsushi Nakanishi,[4] Manabu Oyama,[5] Hitoshi Osaka,[6] Ken Inoue,[7] Kazutoshi Takahashi,[8] Shinya Yamanaka,[8] Kenjiro Kosaki,[9] Takao Takahashi,[2] and Hideyuki Okano[1,*]

[1]Department of Physiology, School of Medicine, Keio University, 35 Shinanomachi, Shinjuku-ku, Tokyo 160-8582, Japan
[2]Department of Pediatrics, School of Medicine, Keio University, 35 Shinanomachi, Shinjuku-ku, Tokyo 160-8582, Japan
[3]Department of Neurology, School of Medicine, Aichi Medical University, 1-1 Yazako Karimata, Nagakute, Aichi 480-1195, Japan
[4]Advanced Science Research Laboratories, Takeda Pharmaceutical Company Limited, 26-1 Muraoka-Higashi 2-Chome, Fujisawa, Kanagawa 251-8555, Japan
[5]Department of Dermatology, School of Medicine, Keio University, 35 Shinanomachi, Shinjuku-ku, Tokyo 160-8582, Japan
[6]Department of Pediatrics, Jichi Medical School, 3311-1 Yakushiji, Shimotsuke-shi, Tochigi 329-0498, Japan
[7]Department of Mental Retardation and Birth Defect Research, National Institute of Neuroscience, National Center of Neurology and Psychiatry, 4-1-1 Ogawahigashi-machi, Kodaira-shi, Tokyo 187-8551, Japan
[8]Center for Induced Pluripotent Stem Cell Research and Application, Graduate School of Medicine, Institute for Frontier Medical Sciences, Kyoto University, Kyoto 606-8507, Japan
[9]Center for Medical Genetics, School of Medicine, Keio University, 35 Shinanomachi, Shinjuku-ku, Tokyo 160-8582, Japan
*Correspondence: yohei@a6.keio.jp (Y.O.), hidokano@a2.keio.jp (H.O.)
http://dx.doi.org/10.1016/j.stemcr.2014.03.007

SUMMARY

Pelizaeus-Merzbacher disease (PMD) is a form of X-linked leukodystrophy caused by mutations in the *proteolipid protein 1* (*PLP1*) gene. Although PLP1 proteins with missense mutations have been shown to accumulate in the rough endoplasmic reticulum (ER) in disease model animals and cell lines transfected with mutant *PLP1* genes, the exact pathogenetic mechanism of PMD has not previously been clarified. In this study, we established induced pluripotent stem cells (iPSCs) from two PMD patients carrying missense mutation and differentiated them into oligodendrocytes in vitro. In the PMD iPSC-derived oligodendrocytes, mislocalization of mutant PLP1 proteins to the ER and an association between increased susceptibility to ER stress and increased numbers of apoptotic oligodendrocytes were observed. Moreover, electron microscopic analysis demonstrated drastically reduced myelin formation accompanied by abnormal ER morphology. Thus, this study demonstrates the involvement of ER stress in pathogenic dysmyelination in the oligodendrocytes of PMD patients with the *PLP1* missense mutation.

INTRODUCTION

Analysis of differentiated cells from disease-specific, human induced pluripotent stem cells (iPSCs) enables the construction of pathological models using the patients' own cells. Such analyses are particularly useful for the study of neurodegenerative disorders because it is difficult to collect brain-tissue samples from these patients.

Pelizaeus-Merzbacher disease (PMD) is a dysmyelinating disorder of the CNS that is usually observed during childhood. PMD is classified into two subtypes: the classical and connatal forms. In the classical form, patients usually show a delay in psychomotor development within the first year of life but exhibit relatively slow disease progression over the first decade. In contrast, in the connatal form, patients generally show arrested congenital psychomotor development and exhibit a progressive disease course with severe neurological impairment. The degree of dysmyelination has been shown to correlate well with the clinical severity of PMD (Seitelberger, 1995). The *proteolipid protein 1* (*PLP1*) gene has been identified as a causative gene for PMD. PLP1 is a transmembrane protein that is abundantly expressed in compact myelin in oligodendrocytes (OLs) and plays a structural role in the formation and maintenance of myelin sheaths (Gow et al., 1997; Mikoshiba et al., 1991). Three distinct types of *PLP1* mutation have been reported to date: point mutations, duplications, and deletions. Missense mutations in the *PLP1* gene account for 30% of the genetic abnormalities found in PMD patients and are responsible for most of connatal cases. Based on analyses using cell lines transfected with mutant *PLP1* genes (Gow and Lazzarini, 1996) or a mouse model of PMD (the *msd* mouse; Gow et al., 1998), the underlying pathogenesis in most patients with missense mutations is thought to involve the accumulation of misfolded mutant PLP1 proteins in the rough endoplasmic reticulum (ER) (Southwood et al., 2002) and the induction of ER stress, resulting in activation of the unfolded protein response (UPR). Although UPR attenuates general translation to reduce the protein load into ER and increase expression of chaperone proteins to facilitate protein folding, excessive levels of unfolded proteins have been shown to activate apoptotic pathway of UPR to eliminate damaged OLs.

However, despite the precise analyses conducted using conventional cellular and animal PMD models, it has not been possible to examine the actual correlation between the known molecular pathogenesis and cell biological phenotypes, including abnormalities in OL differentiation, myelination, and cell death. In addition, those previous results were obtained through analyses using nonhuman models, non-patient-derived cells, or nonoligodendrocyte models, and it is unknown whether the results obtained in those models are applicable to human patients. Although the establishment of iPSCs from a PMD patient with partial duplication of *PLP1* gene has been reported, those iPSCs were not differentiated into oligodendrocytes for disease modeling (Shimojima et al., 2012). Thus, in the present study, we focused on the pathologic effects of *PLP1* missense mutations and established patient-specific iPSCs from two PMD patients with different mutation sites and different levels of clinical severity.

We differentiated the iPSCs into OL lineage cells and examined the pathogenic changes in the PMD iPSC-derived OLs. We confirmed the accumulation and mislocalization of mutant PLP1 proteins to the ER, a high level of stress susceptibility, and increased apoptosis in PMD iPSC-derived OLs. In addition, through transmission electron microscopic analysis, we verified decreases in the frequency of myelin formation and the thickness of the myelin sheath compared with control cells. More importantly, we also demonstrated that these pathogenic changes observed in iPSC-derived OLs were consistent with the different levels of clinical severity between the two PMD patients. Thus, this report describes the modeling of human PMD with *PLP1* missense mutations using patient-specific, iPSC-derived OLs. These results have demonstrated the usefulness of iPSC-derived OLs for the analysis of the pathogenic processes in human dysmyelinating neurological disorders.

RESULTS

Clinical Features of PMD Patients

We established iPSCs from two patients with point mutations in the transmembrane domain (patient 1: PMD1) and extracellular domain (patient 2: PMD2) of the *PLP1* gene (Figure 1C). PMD1 was a 1-year-old male with the connatal form of PMD. He was diagnosed with PMD at the age of 4 months, when he was found to exhibit poor head control and nystagmus and was unable to follow objects. He showed poor feeding and was fed through a gastrostomy tube from the age of 21 months. Psychomotor development was not observed, even at the age of 5 years. MRI of the patient's brain revealed mild and diffuse atrophy, dilatation of the ventricles, and diffuse high-intensity signals in the white matter of the cerebrum and brainstem in a T2-weighted image (T2WI) (Figure 1A). A direct sequencing analysis of genomic DNA from the patient's leukocytes showed a novel missense mutation, c.757 T > A (p.Ser253Thr), in exon 6 of the *PLP1* gene (Figure 1B). This amino acid change has not been previously reported, but different type of mutation at this same site, Ser253Phe, has been reported in other patients with the connatal form of PMD (Hodes et al., 1998). This change was not identified in more than 200 normal individuals; thus, it was considered to be a causative mutation for PMD.

Patient 2 (PMD2) was a 20-year-old male with the classical form of PMD. He was diagnosed with PMD at the age of 3 months, when he was found to display poor head control and nystagmus. Spastic quadriparesis was evident at 4 years of age, with choreoathetotic movements beginning at the age of 8–10 years. He appeared alert and attentive and was nonverbal but exhibited guttural vocalizations. A missense mutation, c.643 C > T (p.Pro215Ser), was identified in exon 5 of the *PLP1* gene, which has been reported previously (Gencic et al., 1989).

Establishment and Characterization of iPSCs Derived from PMD Patients

Human iPSCs were established via the retroviral transduction of four transcription factors (*SOX2*, *OCT4*, *KLF4*, and *c-MYC*) into dermal fibroblasts (Takahashi et al., 2007). A total of 52 and 34 iPSC clones were established from PMD1 and PMD2 samples, respectively. The established iPSC clones were evaluated based on the typical morphology of colonies similar to human embryonic stem cells (ESCs), as well as the expression of pluripotent markers via immunocytochemistry (NANOG and OCT4; Figure 1D), silencing of retroviral transgenes through quantitative RT-PCR (Figure 1E), and efficient differentiation into neural cells via embryoid body (EB) formation. We finally selected three clones each for PMD1 (1-7, 1-15, and 1-27) and PMD2 (2-6, 2-10, and 2-22) for further analyses. The differentiation potentials of these selected iPSC clones were confirmed through teratoma formation assays (ectoderm: neural rosettes and pigmented epithelium, endoderm: goblet cells, and mesoderm: bones and cartilage; Figure 1F). Moreover, the mutations in the *PLP1* gene (PMD1 [c.757 T > A] and PMD2 [c.643 C > T]) were confirmed in human dermal fibroblasts (HDFs) and all of the selected iPSC clones via pyrosequencing analysis (Figure 1G).

Regarding the control iPSCs, we used age-matched control iPSCs established from 8-month-old (TIG121) and 16-year-old (WD39) healthy individuals, corresponding to the PMD-iPSCs established from 1-year-old and 20-year-old patients, respectively, as well as 201B7, which is a widely used control iPSC clone.

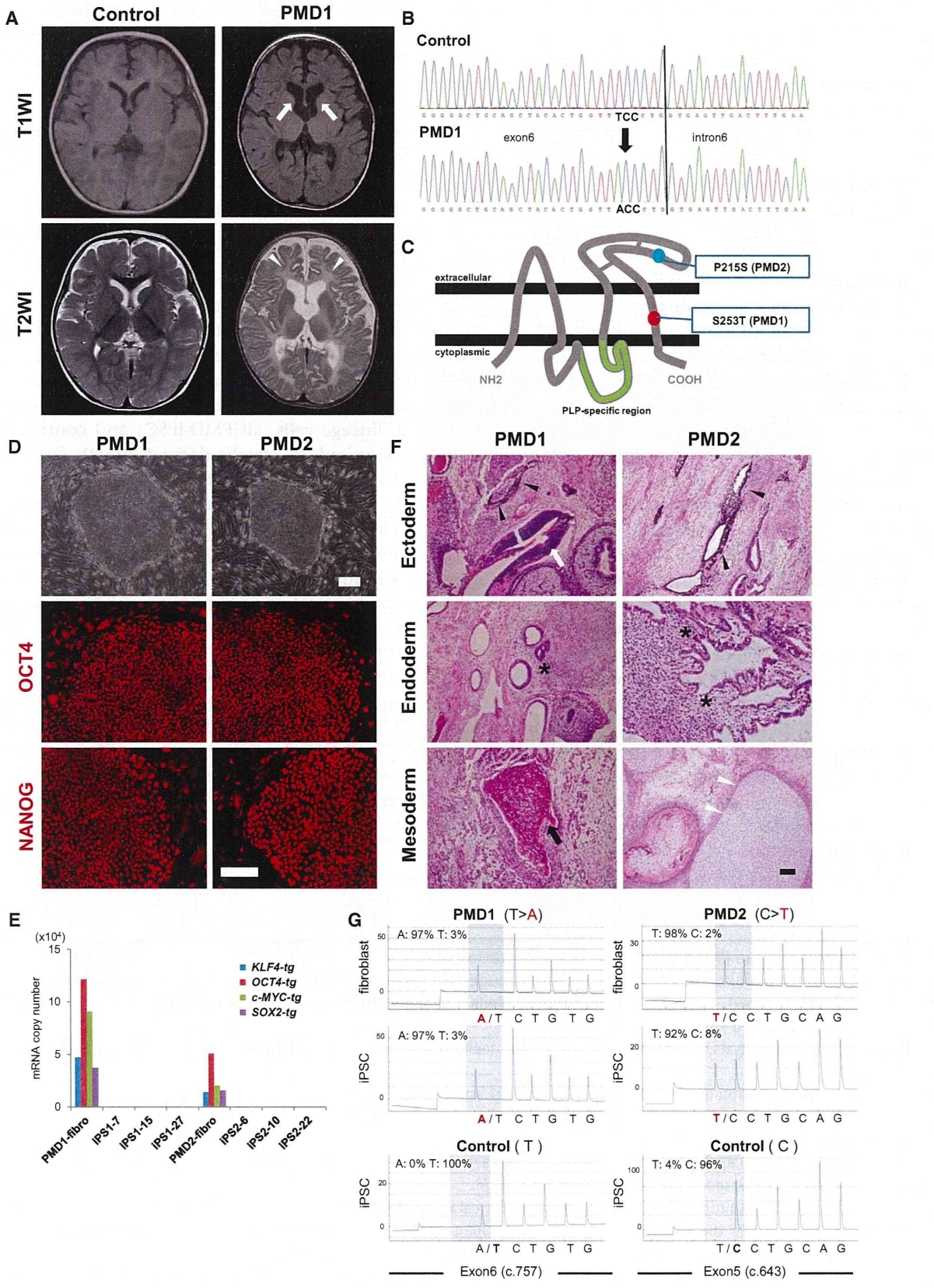

(legend on next page)